The application of estimated sea floor dynamics to improve the resurvey policy of the Netherlands Hydrographic Service

L. L. Dorst, P. C. Roos and S. J. M. H. Hulscher

August 8, 2010

Abstract

Bathymetric resurveying at sea is a costly process with limited resources, yet necessary for adequate nautical charts and therefore crucial for safe navigation. An important factor in an efficient resurvey policy is the type and size of sea floor dynamics. By formulating four indicators, we make recommendations for the resurvey policy of the Hydrographic Service of the Royal Netherlands Navy on the Belgian and Netherlands Continental Shelf. The continental shelf of these two countries is characterized by a sandy sea floor covered with rhythmic patterns and by limited depth. These indicators follow from the estimates for sea floor dynamics, as given by applying the statistical method of deformation analysis. We present a concept for the shallowest likely depth surface, on which we base two of the indicators. The other two indicators act as a warning: they quantify the potentially missed dynamics, which makes the procedure more robust in case of complicated morphology. We show clear differences in recommended resurvey priority between the five analyzed regions, which currently have equal resurvey frequencies.

keywords: deformation analysis, marine morphodynamics, bathymetric surveying, sand waves, maritime navigation

1 Introduction

The Hydrographic Service of the Royal Netherlands Navy (RNLN) is the Dutch government office responsible for nautical surveying and charting, in order to ensure the safety of navigation at sea. To guarantee the presence of accurate information on e.g. depth on board, the usage of official nautical charts is mandatory for many types of ships. Nautical charts are based on bathymetric surveys at sea, which is costly information that expires after limited time, because of the changing nature of the sea floor in many sandy shallow seas. Especially tidal sand waves, which are rhythmic patterns that are widely present on the Belgian and Netherlands Continental Shelf (BNLCS), show dynamics for large parts of the Southern North Sea. Tidal sand waves are characterized by wavelengths of hundreds of meters and amplitudes of up to several meters.

In order to manage bathymetric resurveys efficiently, it is necessary to plan the deployment of the two hydrographic survey vessels of the Royal Netherlands Navy according to a carefully designed resurvey policy. The policy assigns a resurvey frequency to all areas of the BNLCS under RNLN responsibility. The current policy is given in Figure 1. Due to various circumstances, the RNLN has not achieved these resurvey frequencies over the past years, which makes the justification of those frequencies by a comprehensive risk assessment even more relevant [*Dienst der Hydrografie*, 2007].

Hydrographic offices around the world are considering ways to specify resurvey frequencies for shipping routes in shallow waters. Survey policies are made worldwide, and published on the internet [*NOAA Office of Coast Survey*, 2008] or in the literature [*De Oliveira et al.*, 2007; *Dehling*, 2006; *Whatrup et al.*, 2005]. Ideally, the resurvey frequencies of a policy are based on five factors:

1. minimum depth;
2. draught, i.e. the depth of a ship's keel under sea level;
3. shipping intensity;
4. human interventions;
5. sea floor dynamics.

Areas that are deeper than necessary for any surface navigation do not need to be monitored as often as shallower areas (factor 1). The distinction between shallow and deep usually lies at 40 m [*International Hydrographic Organization*, 2008a]. Draught (factor 2) often is most critical in shipping lanes, which are potentially maintained at a larger depth than the surrounding sea floor.

Shipping intensity (factor 3) is important because of its direct impact on the grounding risk in case of sea floor changes, and because it is a cause of changes in depth in itself. Intense shipping increases the risk of cargo loss (like containers), which enlarges the probability of undetected objects on the sea floor. Human intervention in the natural processes of shallow sandy seas (factor 4) include dredging, sand mining and dumping, land reclamation, and the placement of objects on the sea floor (like wind farms) [*Van der Veen*,

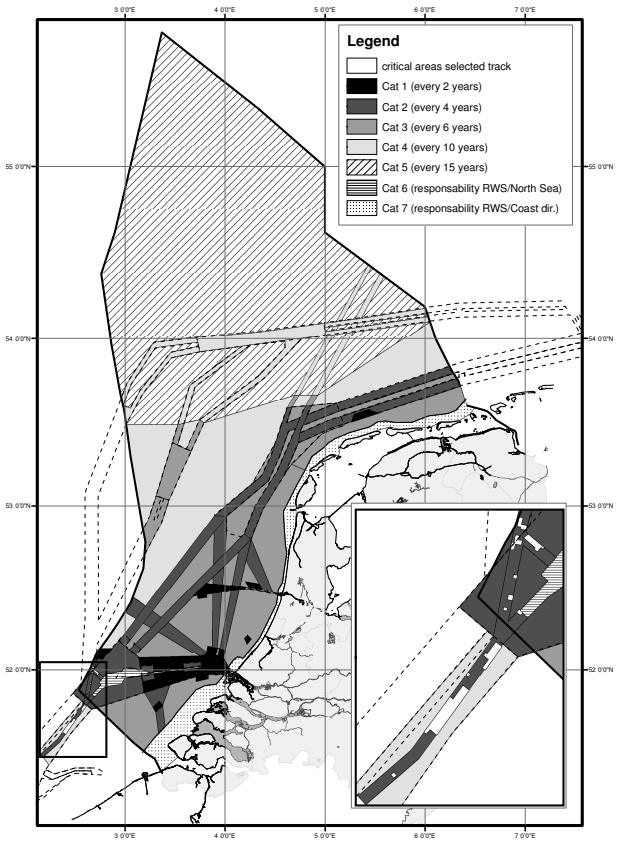

Figure 1: The 2003 resurvey policy of the Hydrographic Service of the Royal Netherlands Navy, for the areas of the Belgian and Netherlands Continental Shelf (BNLCS) under its responsibility. In the Selected Track for deep draught vessels, Critical areas are defined that have a resurvey frequency of once every two years. The Hydrographic Service does not survey the areas that are under responsibility of Rijkswaterstaat North Sea, or their coastal directorates. (Figure courtesy of Lt I.J. Nijman)

2008; *Roos et al.*, 2008]. Human intervention in natural processes also have an indirect effect that may cause long-term changes in depth until tens of kilometres away from the location of the intervention.

Present morphodynamic models allow for the qualitative prediction of the effect of human intervention in the natural morphological processes, like areas where accretion or removal of sediment is expected [*Van der Veen*, 2008; *Roos et al.*, 2008], or sand wave growth and migration [*Besio et al.*, 2008; *Németh et al.*, 2007]. This knowledge gives opportunities to adapt resurvey frequencies based on human interventions, past or planned, in combination with observed sea floor dynamics (factor 5). This study presents a systematic way to use knowledge of sea floor dynamics to optimize the resurvey policy. Although several strategies currently are in use, a newly developed method known as deformation analysis [*Dorst et al.*, 2009] gives new opportunities.

Starting with *Langeraar* [1966], attempts have been made to quantify dynamics of the Southern North Sea for this purpose. The most recent estimates are given in *Dorst* [2009], using deformation analysis. This method is based on statistical testing theory, and is able to estimate dynamics of the sea floor using just a few morphological parameters and their uncertainties. These estimates include the behaviour of tidal sand waves. However, the estimates of deformation analysis are not directly useful to recommend changes in resurvey frequency. Therefore, we formulate a set of indicators that enables prioritization of areas with respect to each other, for sea floor dynamics. This serves as input for a future scientific validation of the resurvey policy [*Deltares*, 2008].

Because of the differences in present and past resurvey frequency between the areas, the number of available surveys and the time interval of the analyses varies. Also, the morphology varies between the areas. This complicates the comparison of detected depth reductions between the areas. To remove these complications, we use observed shoaling rates, instead of observed depth differences between surveys. We reduce the resulting morphological parameters and their uncertainty to just two indicators for detected behaviour of an area.

We add another two indicators for the risk of missed dynamics to the procedure, which is necessary because some dynamics are potentially too small to be detected, given the uncertainty of the results. This is especially important because the uncertainty of areas that are showing more irregular sand wave patterns will in general be higher than the uncertainty of areas for which sand wave patterns are absent or less irregular.

First, current practice on relevant aspects of hydrography, e.g. strategies to include sea floor dynamics in resurvey policies, are given in Section 2. Then, four indicators for the interpretation of sea floor dynamics are introduced in Section 3. Indicator values for the results of the analyzed areas in the Southern North Sea are presented in Section 4. In Section 6, we discuss our findings in relation to other hydrographic and morphological concepts, and make recommendations for the resurvey policy of the Netherlands Hydrographic Service, using current hydrographic practice and the indicator results in our discussion. We finish with some conclusions in Section 7.

2 Background: Hydrographic practice

2.1 Manual and automatic shoal biasing

Traditionally, depth values used for nautical publications are made shallower, and thereby safer, using manual *shoal biasing*. Only the shallowest depth values are depicted, assuming they are representative for the shallowest value that could be present at any nearby location. Also, the *isobaths*, which are contour lines of equal depth, are *generalized* (i.e. cartographically smoothed), dependent on the scale, towards the shallow direction only. In this process, the experience of the cartographer plays a central role.

Recently, an alternative approach to shoal biasing was proposed, known as the *navigation surface* [*Smith*, 2003; *Smith et al.*, 2002]. The approach of the navigation surface is algorithmic, which enables automatic processing, and thus decreases the processing time of very large MBES data sets. Also, this approach removes subjectivity from the processing of bathymetric surveys. The procedure uses depth values and their uncertainty at a grid of nodes, generated by the Combined Uncertainty and Bathymetry Estimator (CUBE) [*Calder*, 2003], or potentially by Kriging [e.g. *Dorst*, 2009; *Calder*, 2006].

In the navigation surface approach, isobaths are generated by *defocusing* using a *double buffering* algorithm, which generates a line at a constant distance in the deeper direction, and subsequently generates the generalized line at the same distance in the opposite direction. The constant defocusing distance is scale-dependent, allowing for various levels of generalization.

2.2 Inadequately surveyed areas

The major part of the marine environment has never been adequately surveyed . Even major international shipping routes have not been surveyed according to modern standards [*International Hydrographic Organization*, 2008b]. Therefore, only the resources that are necessary to resurvey previously surveyed areas should be spent, making more resources available to survey other areas.

To mitigate the influence of inadequately surveyed areas, various methods have been developed to indicate the quality of the survey to the mariner [*Heap*, 2007]. The most recent development is the introduction of zones of confidence (ZOC) of the nautical chart, especially feasible for electronic nautical charts (ENC-s) [*International Hydrographic Organization*, 2007]. However, most of these concepts only focus on the quality and density of the measurements. The aging aspect is not included, as it is impossible to get reliable insight into sea floor changes, without a thorough analysis of a series of previous surveys, or the application of a morphological model. With the introduction of new analysis techniques, like the deformation analysis used in this study, and with the ongoing development of morphological models, the inclusion of the effect of age in a quality indicator becomes possible.

2.3 The inclusion of sea floor dynamics in resurvey policies

Among hydrographic services, the following strategies are in use to deal with the factor sea floor dynamics in resurvey policies:

1. interpretation of a series of archived bathymetric surveys, as in this study;
2. use of exploratory surveys, in which a small part of an area is measured, and the decision on the resurvey of the whole area is based on the analysis of the exploratory survey;
3. observation of the general morphology of the sea floor, using a remote sensing technique;
4. application of morphodynamic models to predict sea floor change.

The interpretation of a series of bathymetric surveys (strategy 1) is the most traditional method, documented by e.g. *Burton* [1977] and *Kember* [1984]. An example of the application of exploratory surveys (strategy 2) is the measurement of a single survey track over a sand dune [*Le Bot et al.*, 2000].

An example of a remote sensing technique (strategy 3) is the interpretation of radar reflections on surface waves, which are influenced by changes in depth. Radar observations are available from satellites or from terrestrial stations [*Calkoen et al.*, 1998]. Also, water color is an indicator of depth for seas with clear water [*Su et al.*, 2008]. Experiments with radar remote sensing for the North Sea have given results of mixed quality [*Swart et al.*, 2006]. *Kember* [1984] stresses that any review of resurvey frequency should first investigate sea floor changes, preferably quantitatively, and subsequently should attempt to understand the morphological mechanisms (strategy 4) that cause these changes.

3 Method: indicators of sea floor dynamics

3.1 Introduction to deformation analysis

Our application of deformation analysis [*Dorst et al.*, 2009; *Dorst*, 2009] represents the sea floor and its dynamics as a fairly simple characterization by parameters, accompanied by the dispersion of the observed sea floor form this characterization in a covariance matrix. One way to describe the representation is in the

parameter domain, given by the $N \times 1$ vector of estimated morphological parameters $\underline{\hat{\mathbf{u}}}$ and its covariance matrix $\underline{\mathbf{C}}_u$, for the characterization and the dispersion respectively. The main diagonal of $\underline{\mathbf{C}}_u$ contains the variances σ_u^2 of the parameters $\underline{\hat{u}}$. We assume a Gaussian distribution for the deviations described by the dispersion. In vector $\underline{\hat{\mathbf{u}}}$, there are U parameters $\underline{\hat{u}}_{\mathrm{ref}}$ at reference time t_{ref}. Depending on the complexity of the detected dynamics, V dynamic parameters $\underline{\hat{v}}$ follow the reference parameters in $\underline{\hat{\mathbf{u}}}$, with $N = U + V$ and $N \leq US$.

Alternatively, the representation is described in the *depth domain*, given by the $M \times 1$ vector of estimated depth values $\underline{\hat{\mathbf{m}}}$ and and its covariance matrix $\underline{\mathbf{C}}_m$, at the grid nodes $\mathbf{x}_p$. The relation between both the domains is linear [*Dorst et al.*, 2009]:

$$\underline{\hat{\mathbf{m}}} = \mathbf{A}\underline{\hat{\mathbf{u}}}, \quad \underline{\mathbf{C}}_m = \mathbf{A}\underline{\mathbf{C}}_u\mathbf{A}^{\mathrm{T}}, \tag{1}$$

in which $\mathbf{A}$ is an $M \times N$ coefficient matrix.

The representation in the depth domain by $\underline{\hat{\mathbf{m}}}$ and $\underline{\mathbf{C}}_m$ is smoothed with respect to the original surveyed depth values $\underline{\mathbf{d}}$ and $\underline{\mathbf{C}}_d$: the estimation procedure removes residual variations and reduces measurement errors. This is illustrated in Figure 2a. The smoothing of the characterization $\underline{\mathbf{d}}$ to $\underline{\hat{\mathbf{m}}}$ is compensated for by the increase of the dispersion from $\underline{\mathbf{C}}_d$ to $\underline{\mathbf{C}}_m$, which contains a component for the residuals, as in Figure 2b. The variances on the main diagonal of a covariance matrix $\underline{\mathbf{C}}$ are used to construct a confidence interval around the estimates. For the 95% confidence interval, the lower limit at 2.5% is denoted by $\underline{d}_{2.5\%}$ or $\underline{\hat{m}}_{2.5\%}$, and the upper limit at 97.5% by $\underline{d}_{97.5\%}$ or $\underline{\hat{m}}_{97.5\%}$. Analogously, the estimates $\underline{d}$ and $\underline{\hat{m}}$ are denoted by $\underline{d}_{50\%}$ and $\underline{\hat{m}}_{50\%}$.

The more dimensions we use for the representation, the fewer the parameters in the parameter domain. A 0D approach uses the morphological parameters to describe the P nodes of a 2D grid, a 1D approach to describe $\sqrt{P}$ grid lines (if the grid is square and oriented in the direction of highest variability), and a 2D approach uses only one grid. The maximum number of spatial parameters per survey U is one , four and five , respectively. The maximum number of parameters is therefore the number of analyses for a grid times the maximum number of spatial parameters: $P \cdot S$ for 0D, $\sqrt{P} \cdot 4S$ for 1D, and $1 \cdot 5S$ for 2D. As the 2D parameter vector contains fewer parameters, it is unable to represent to same sea floor complexity as the 1D vector, which causes the smoother representation in the depth domain. The 0D representation is able to use the same number of PS parameters as the number of measurements, which means it is able to reproduce the original morphology at its full complexity, if the maximum number of S temporal parameters would be used for all P nodes.

In practice, it is rare that sand wave patterns are regular in a 2D analysis, see e.g. Section 4. This means that the 1D representation approximates the morphology significantly better than the 2D representation. Therefore, we will use the 1D results to calculate indicators for sea floor dynamics, as they give the best combination of small residuals and filtering of small-scale irregularities.

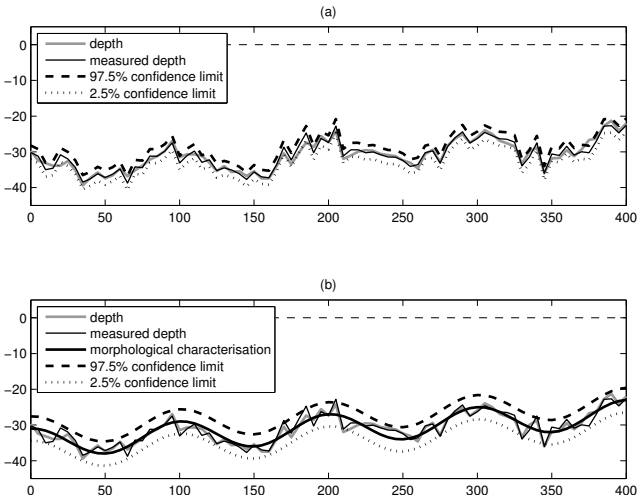

Figure 2: Measured depth $\underline{d}$ in relation to (a) the true, unknown depth d, including the 95% confidence interval around the measured depth, representing the measurement error as described by $\underline{\mathbf{C}}_d$; (b) morphological characterization in the depth domain $\underline{\hat{m}}$ including the 95% confidence interval around the measured depth, representing the measurement error and residual morphology as described by $\underline{\mathbf{C}}_m$. The difference between the measured depth and the characterization is the residual, consisting of a measurement component and usually a morphological component. The probability that the true depth d is larger than the deeper limit of the confidence interval is 2.5% for both $\underline{d}_{2.5\%}$ (graph (a)) and $\underline{\hat{m}}_{2.5\%}$ (graph (b)), and this probability is 97.5% for the shallower limit of both $\underline{d}_{97.5\%}$ (graph (a)) and $\underline{\hat{m}}_{97.5\%}$ (graph (b)).

3.2 Shallowest likely depth values

3.2.1 Prediction

The present resurvey frequency of an area defines the *expected moment of next survey* t_{S+1} as the moment of last survey t_S plus the resurvey period. In practice, it is not always possible to survey according to the planned resurvey frequency. Therefore, the average period between surveys $\bar{T}$ is used as the resurvey period instead:

$$t_{S+1} = t_S + \bar{T}, \quad \bar{T} = (t_S - t_1)/(S-1). \tag{2}$$

To predict the expected sea floor morphology at $t = t_{S+1}$, we apply linear extrapolation. We define the $U \times$

1 vector $\hat{\underline{\mathbf{u}}}_{S+1}$ of predicted morphological parameters as:

$$\hat{\underline{\mathbf{u}}}_{S+1} = \mathbf{F}\hat{\underline{\mathbf{u}}}, \quad \underline{\mathbf{C}}_{u,S+1} = \mathbf{F}\underline{\mathbf{C}}_u\mathbf{F}^{\mathrm{T}}. \tag{3}$$

The $U \times N$ coefficient matrix $\mathbf{F}$ consists of an $U \times U$ identity matrix and an $U \times V$ submatrix for the dynamic parameters in $\hat{\underline{\mathbf{u}}}$. The columns for the outlier estimates $\Delta\underline{u}_s$ are vectors of zeros, and the columns for the trend estimates $\underline{\dot{u}}$ correspond to the vector of time differences $t_s - t_{\mathrm{ref}}$. This means that outliers in the parameters are ignored for the predictions, and trends are linearly extrapolated.

As an example, it follows from equation (3) for the prediction of a parameter u that:

$$\hat{\underline{u}}_{S+1} = \begin{cases} \underline{\hat{u}}_{\mathrm{ref}} & (\text{if } u \text{ static}) \\ \underline{\hat{u}}_{\mathrm{ref}} + (t_{S+1} - t_{\mathrm{ref}})\hat{\underline{\dot{u}}} & (\text{if } u \text{ dynamic}). \end{cases} \tag{4}$$

Correspondingly, the variance of the predicted parameter $\hat{\underline{u}}_{S+1}$ is:

$$\underline{\sigma}^2_{u,S+1} = \begin{cases} \underline{\sigma}^2_{u,\mathrm{ref}} & (\text{if } u \text{ static}) \\ \underline{\sigma}^2_{u,\mathrm{ref}} + (t_{S+1} - t_{\mathrm{ref}})^2\underline{\sigma}^2_{\dot{u}} & (\text{if } u \text{ dynamic}). \end{cases} \tag{5}$$

If no trend has been detected for the parameter u, the estimates $\hat{\underline{u}}_{S+1}$ and their variances $\sigma^2_{u,S+1}$ are static, i.e. independent of the moment of prediction t_{S+1}. If the value of a parameter contains a trend, the variances $\sigma^2_{u,S+1}$ increase in time.

The $P \times U$ coefficient matrix $\mathbf{A}_{S+1}$ describes the relation between the predicted representations in the parameter domain and the depth domain. The elements of $\mathbf{A}_{S+1}$ correspond to the elements in the first U columns of $\mathbf{A}$. The predicted representation in the depth domain follows from the predicted representation in the parameter domain according to:

$$\hat{\underline{\mathbf{m}}}_{S+1} = \mathbf{A}_{S+1}\hat{\underline{\mathbf{u}}}_{S+1}, \quad \underline{\mathbf{C}}_{m,S+1} = \mathbf{A}_{S+1}\underline{\mathbf{C}}_{u,S+1}\mathbf{A}^{\mathrm{T}}_{S+1}. \tag{6}$$

The extended representation in the depth domain contains the representations for all the surveys s, and the predicted representation. It is denoted $\hat{\underline{\mathbf{m}}}^+$ and $\underline{\mathbf{C}}^+_m$ for its $P(S+1) \times 1$ characterization vector and $P(S+1) \times P(S+1)$ covariance matrix.

3.2.2 Depth reduction

The crucial property of a bathymetric representation for maritime navigation is the shallowest depth that is expected. Depth is already reduced for the water level above the reference low-water surface, during the processing of the survey. We reduce it further to create a safe margin for navigation in areas that are potentially dynamic. For this reduction, we use the extended representation in the depth domain. We assume a Gaussian distribution for the deviations, as described by the dispersion, and specify a 97.5% confidence level to the requirement that the depth should not be shallower than given by the representation.

This enables us to compute a depth-reduced characterization:

$$\hat{\underline{\mathbf{m}}}^+_{97.5\%} = \hat{\underline{\mathbf{m}}}^+ - 1.96\sqrt{\mathrm{diag}(\underline{\mathbf{C}}^+_m)}. \tag{7}$$

The operator diag() converts the main diagonal of the covariance matrix into a column vector of variances. We regard it *unlikely* that the true depth d is shallower than its element in $\hat{\underline{\mathbf{m}}}^+_{97.5\%}$, as depicted by the upper confidence limit in Figure 2b. Therefore, the vector $\hat{\underline{\mathbf{m}}}^+_{97.5\%}$ contains the *shallowest likely depth values*. It represents the $S+1$ shallowest likely depth surfaces $\hat{\underline{m}}_{97.5\%}(x, y)$.

3.3 Two indicators for rates of change

3.3.1 The creation of a bias in the shallow direction

For a static sea floor, the estimated depth values and uncertainties are constant. Consequently, the shallowest likely depth values are constant, and therefore their rates of change are zero.

For a dynamic sea floor, the predicted depth values $\hat{\underline{\mathbf{m}}}_{S+1}$ are likely to have the largest uncertainty. This means for the rates that the addition of the prediction creates a bias towards the shallow direction, shown in Figure 3. The less frequent a resurvey is done, the larger the time span of the prediction becomes. Large predictive time spans relative to the size of a trend result in a larger positive bias of the shoaling rate. This makes a rate a valuable indicator for the necessity to change the resurvey frequency of an area, in comparison to other areas.

3.3.2 The shallowest likely depth rate

For a mariner, it is not important to know where exactly the shallowest likely depth is located. Instead, it is important to know what the *overall shallowest likely depth* is of the whole area, and how this depth evolves in time. Therefore, we select the minimum over the P depth values in subvector $\hat{\underline{\mathbf{m}}}^+_{97.5\%,s}$ per survey s.

We use these $S+1$ overall shallowest likely depth values for a least-squares estimation of their rate of change in a linear regression analysis, using the variances of the corresponding depth values $\hat{\underline{m}}^+_{p,s}$ as weights. The result is the *shallowest likely depth rate* (SLDR), depicted in Figure 4. Because the variances of the depth values are used for the estimation of the SLDR, a variance is associated with it, describing its uncertainty. Also, we calculate a correlation coefficient $\rho^{(\mathrm{S})}$ to express the deviations of the shallowest likely depth values from the estimated linear rate.

3.3.3 The maximum estimated shoaling rate

To decide whether a resurvey is necessary, the shallowest likely depth in an area alone is not sufficient. In ad-

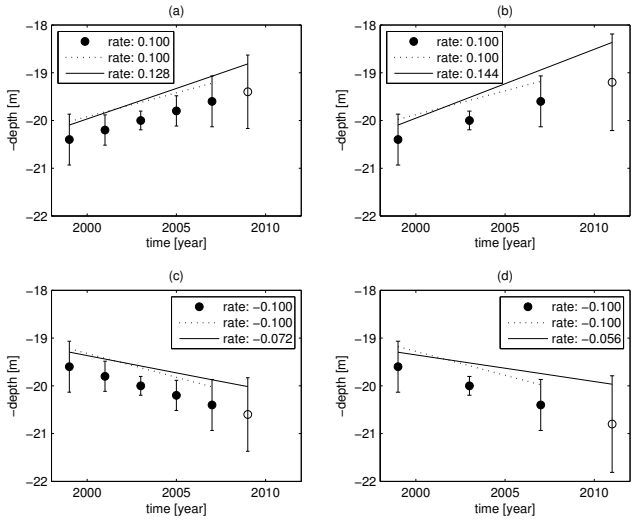

Figure 3: Creation of a bias in a rate of change of the shallowest likely depth, by adding a prediction (white circle) to the survey moments (black circles): (a) depth decrease, two year resurvey frequency; (b) depth decrease, four year resurvey frequency; (c) depth increase, two year resurvey frequency; (d) depth increase, four year resurvey frequency.

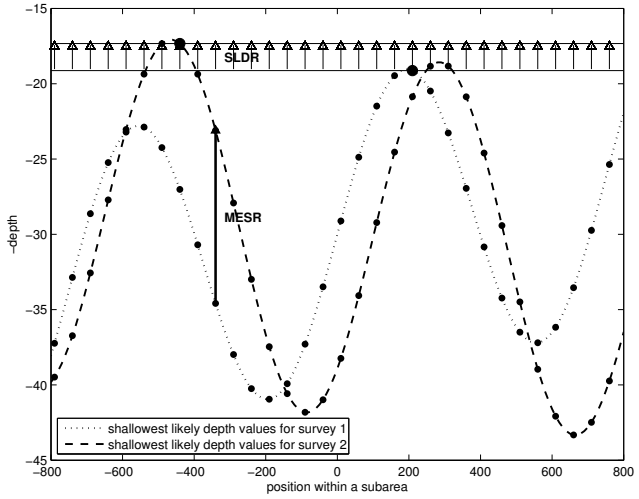

Figure 4: The calculation of the SLDR and MESR from the shallowest likely depth values of two surveys, measured a year apart. The SLDR is based on the overall shallowest likely depth values of each survey, indicated by the larger black circles, while the MESR is the maximum of the rates of the shallowest likely depth values at the grid nodes.

dition, the *shoaling rate* at any point p within the area is necessary information. The decision if a shallower depth is relevant does not only depend on its position on top of or away from a sand wave crest, but also on the chart scale. The SLDR does not detect a migration of the shallowest likely depth, which is important information for the update of detailed charts. Therefore, we estimate a rate of change at each grid node, using the $S+1$ depth values in subvector $\underline{\hat{\mathbf{m}}}^{+}_{97.5\%,p}$.

Again, we perform least-squares estimations of the rates of change, by calculating a linear regression per grid node with the variances as weights. We regard it unlikely that the true shoaling rate at any position within the area is larger than the *maximum estimated shoaling rate* (MESR) of the shallowest likely depth values for the 97.5% confidence level at the grid nodes $p = 1, \cdots, P$. The MESR is also depicted in Figure 4. Because the variances of the depth values are used for the estimation of the MESR, a variance is associated with it, describing its uncertainty. Also, we calculate a correlation coefficient $\rho^{(\mathrm{M})}$ to express the deviations of the shallowest likely depth values from the estimated linear rate.

3.4 Two indicators for the risk of missed dynamics

3.4.1 Introduction

Deformation analysis is able to detect smaller dynamics for less irregular sand waves, as those sand waves are represented better by the estimated parameters. In that case, the residuals are smaller, resulting in smaller detectable spatial and dynamic parameters. It also results in smaller variations between the parameter estimates and in parameter existence between the areas. A quantification of the *irregularity* of sand waves would therefore be a valuable predictor for the performance of our implementation of deformation analysis. In the determination of sand wave irregularity, it is helpful to distinguish between irregularities that are caused by the shape of the pattern in x-direction and irregularities caused by the continuation of the pattern in y-direction. We term the first type *wave irregularity* and the second type *crest irregularity*. We define one-dimensional sand wave irregularity as the difference with the estimated sinusoidal wave in the direction across the crest. This difference is given by a variable for the size of the morphological residuals, as explained in more detail below. Two-dimensional irregularity also contains the variation of the sand wave pattern in the direction along the crest.

Two types of wave irregularity are distinguished: *horizontal wave asymmetry* (also lee-stoss asymmetry and skewness) and *vertical wave asymmetry* (also crest-trough asymmetry and peakedness) of the sand wave pattern. Horizontal asymmetry is explained by residual currents or by tidal asymmetry [*Besio et al.*, 2008;

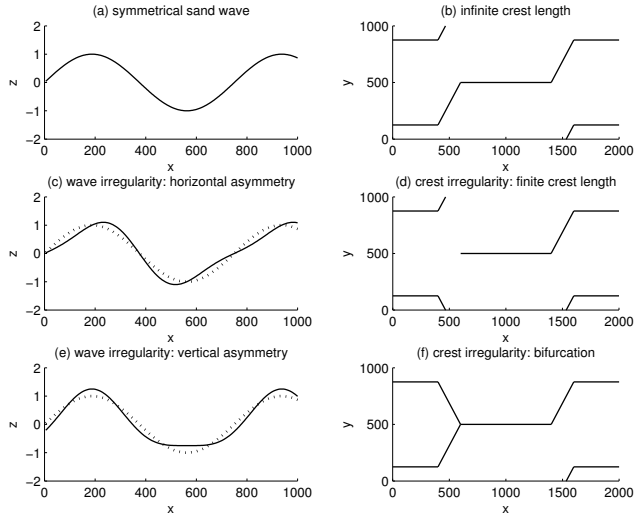

Figure 5: Wave irregularity shown by depth values in an (x,z) coordinate frame (left) and crest irregularity shown by crest positions in an (x,y) coordinate frame (right). The graphs on the left show: (a) wave symmetry; (c) horizontal asymmetry (skewness); and (e) vertical asymmetry (peakedness) of the crests. The graphs on the right show: (b) shifting crest segments (d) finite-length crests; and (f) bifurcations. In the graphs (c) and (e), the original symmetrical sand wave is shown dotted.

Németh et al., 2007], and indicates migration of the pattern [*Knaapen*, 2005]. Crest irregularities include shifting crest segments, bifurcations and finite-length crests. They could be explained by differences in migration rate between parts of the pattern, e.g. as a result of differences in depth [*Dorst*, 2009]. Examples of these irregularities are given in Figure 5.

A first distinction between regular and irregular sand waves is made using the overall test quotient. To enable a comparison between areas, we subsequently quantify the degree of irregularity, for which we use the morphological variance. Finally, the effect of irregularity on the minimal detectable dynamics is illustrated. The minimal detectable dynamics are necessary to interpret the results, used to adapt the resurvey policy.

3.4.2 Regular versus irregular sand wave patterns

The sinusoidal sand wave extension of step 1 in the deformation analysis procedure [*Dorst et al.*, 2009] represents a perfectly regular sand wave. This step selects the required spatial parameters by adding extensions to the morphological characterization. The differences between the characterization and the measurements are the estimated residuals, in vector $\underline{\hat{\mathbf{r}}}$. In this first step, the overall test quotient $\underline{q}^{(\mathrm{o,m})}$ represents the size of the square of the estimated residuals in relation to the measurement and interpolation uncertainty, which is described by covariance matrix $\mathbf{C}_d$. Therefore, the overall test quotient expresses how much of the differences between the measured pattern and the best approximation by a sinusoidal wave could be due to the measurement and interpolation error $\underline{e}$, and how much of that difference remains to be explained as sand wave irregularity.

An area for which the overall test quotient $\underline{q}^{(\mathrm{o,m})} \leq 1$ is called *regular*: all residual variation can be explained by the measurement and interpolation uncertainty. If $\underline{q}^{(\mathrm{o,m})} > 1$, it is called *irregular*, because a part of the residual variation has to be explained by morphological deviations from the sinusoidal sand wave characterization.

3.4.3 The degree of irregularity of a pattern

The initial covariance matrix of step 1 only contains values for the measurement and interpolation errors, and is denoted $\mathbf{C}_d^{(\mathrm{e})}$. After the Least-Squares Variance Component Estimation (LSVCE) [*Dorst et al.*, 2009], the covariance matrix also contains morphological covariance components. These additional components are given in covariance matrix $\mathbf{C}_d^{(\mathrm{m})}$, and summed to obtain the final covariance matrix $\mathbf{C}_d^{(\mathrm{em})}$ of step 1.

The presence of small-scale morphological variations, like mega-ripples, possibly differs per survey, due to e.g. extreme meteorological events, and consequently we need to make a distinction between the morphological components per survey as well, denoted $\underline{\mathbf{C}}_{d,k}^{(\mathrm{m})}$, for $k = 1, \cdots, S$. All variance values on the main diagonal of such a covariance matrix are assumed equal, and estimated as variance factors $\hat{\underline{\sigma}}_s^{(\mathrm{m})2}$ from the residuals, using a least-squares procedure [*Dorst et al.*, 2009]. The morphological variance factors resulting from the one-dimensional analyses give us the wave irregularity, and the two-dimensional morphological variance factors include the influence of both wave and crest irregularity.

3.4.4 The effect of irregularity on the detection of dynamics

To quantify the dynamics that can still be found in the presence of a certain irregularity, we calculate the size of dynamics $|v_a|$ that are *minimal detectable*, as a function of the morphological variance. These dynamics are called *Minimal Detectable Biases* (MDB-s), which are detectable with a percentage γ that is known as the power. Analogously to *Dorst* [2009], we use a power γ of 50%, to obtain the dynamics that are as often detected as they are not. Larger dynamics, or biases, can be detected with a higher probability than γ, and smaller biases with a smaller probability. Even a very small bias can be found, with a small probability, but a very large bias will remain undetected with a certain small probability as well. We also use a power

Table 1: Values of one-dimensional and two-dimensional MDB-s for the detection of dynamics in step 2. The MDB-s are given for a defined morphological variance $\sigma^{(m)2}$ of 0.1, 1, and 10 m^2, for a new survey, two years after the sixth.

type of dynamics	$\sigma^{(m)2}$ [m^2]	MDB (1D) γ=50%; 95%	MDB (2D) γ=50%; 95%	
linear	0.1	0.03; 0.06	0.007; 0.013	m/2yr
trend	1	0.10; 0.19	0.02; 0.04	m/2yr
in depth	10	0.31; 0.59	0.07; 0.13	m/2yr
outlying	0.1	0.21; 0.39	0.05; 0.09	m
depth	1	0.50; 0.92	0.11; 0.21	m
	10	1.53; 2.80	0.34; 0.63	m
linear	0.1	0.04; 0.08	0.009; 0.017	m/2yr
trend	1	0.13; 0.25	0.03; 0.06	m/2yr
in amplitude	10	0.40; 0.77	0.09; 0.17	m/2yr
outlying	0.1	0.28; 0.52	0.06; 0.12	m
amplitude	1	0.66; 1.21	0.15; 0.27	m
	10	1.99; 3.66	0.45; 0.82	m

of 95%, to compare the MDB-s to depth uncertainty at a 95% confidence interval.

Examples of the values of the dynamics that are minimal detectable are given in Table 1. The coefficient matrix **A** is specified using the following details: for the one-dimensional MDB-s, a grid line of twenty nodes is defined, and for the two-dimensional MDB-s, the grid has a size of twenty times twenty nodes; the grid spacing is 50 m; six surveys in ten year are done; a sinusoidal sand wave with a wavelength of 750 m is present; there are no other sea floor dynamics than the single type that is specified. The constant error variance $\sigma^{(e)2}$ is set at 0.1 m^2.

Because of the absence of covariances for the MDB calculation, we should expect that these MDB-s are not detected with the specified power in reality. Nevertheless, Table 1 illustrates that trends are easily detectable, also for larger morphological variances and the one-dimensional grid line analysis. Table 1 also illustrates that outlying values are much harder to detect, in the cases of a relatively large morphological variance. Also, it is clear that it is about twice as hard to detect dynamics with a power of 95% than with a power of 50%.

As Table 1 already illustrates, the outlying sand wave amplitude is the hardest type of dynamics to detect. Because we hardly found any amplitude growth in the studied regions [*Dorst*, 2009], and migration does not affect the overall shallowest likely depth values, we instead use the MDB-s for a depth outlier as indicators.

It is also clear from Table 1 that more dynamics can be detected by a two-dimensional grid analysis than by a one-dimensional grid line analysis, provided that the specified dynamics are constant over the grid. As shown in *Dorst* [2009], for some subareas dynamics are found for several grid lines, while the grid analysis does not show dynamics. Because bed level dynamics are in practice not always constant over a grid, but also often do not happen in specific directions only, we use both the one-dimensional and the two-dimensional MDB-s as indicators. A power γ of 95% is chosen, to allow for a comparison with the 95% confidence interval for depth uncertainty, as specified by S44, for the appropriate order and at the observed bed level [*International Hydrographic Organization*, 2008a].

3.5 Combination of the four indicators

In this Section, we describe how we combine the four indicators introduced previously: SLDR, MESR, 1D MDB, and 2D MDB. The two indicators SLDR and MESR work well in combination: in the calculation of the SLDR, spatial differences are eliminated first, and the rate of change for a grid is estimated next. In contrast, the calculation of the MESR first estimates rates of change at each node, and space is eliminated next. These properties cause sand wave growth to dominate the SLDR, and sand wave migration to dominate the MESR. The MDB indicators are a useful addition, because they provide an extra warning against dynamics that are potentially missed by the first two indicators.

An indicator is termed large if it exceeds a critical value. For the SLDR and the MESR, the critical values are their uncertainties at a 95% level. For the MDB-s, we use vertical uncertainties as stated by the IHO S44 standards, which are depth-dependent.

We use the following priority scheme.

1. Assign first priority to areas that have large positive SLDR-s, because the minimum depth values decrease for those areas.

2. Assign second priority to the other areas that have large positive MESR-s, because there are locations within those areas where the depth values decrease.

3. Assign third priority to the other areas that have large two-dimensional MDB-s, because large-scale dynamics of significant size could be missed in those areas.

4. Assign fourth priority to the other areas that have large one-dimensional MDB-s, because small-scale dynamics of significant size could be missed in those areas.

5. Assign fifth priority to all other areas.

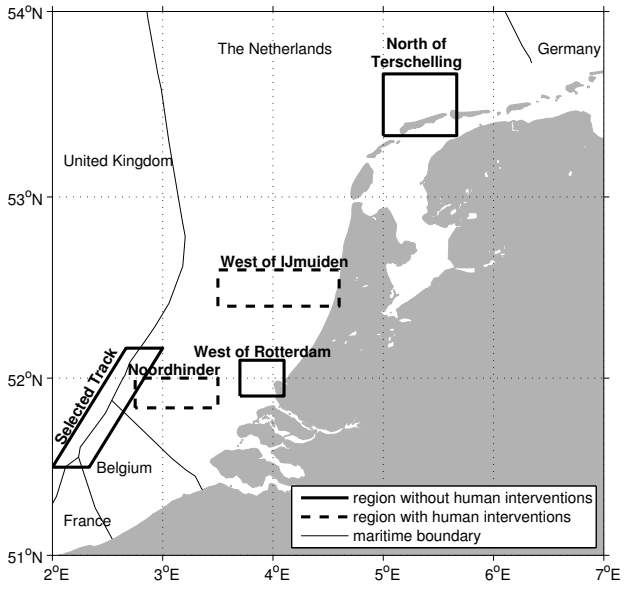

Figure 6: Overview of analyzed regions on the Belgian and Netherlands Continental Shelf.

4 Results: indicator values for the Southern North Sea

4.1 The two rates of change

The morphodynamics of five regions in the Southern North Sea have been estimated using deformation analysis. Results are given in *Dorst* [2009] for five different regions. The regions are shown in Figure 6, and the areas per region are listed in Table 2. Areas are subdivided into subareas, for each of which a grid is available.

An overview of the resulting indicators SLDR and MESR is given in Table 3. The SLDR values are all close to zero, meaning that the shallowest likely depth values per subarea hardly change. Exceptions are the SLDR values for the SBES surveys of the Noordhinder Junction, as it indicates that the shallowest likely depth per subarea is increasing. This confirms the results for those surveys [*Dorst*, 2009]. The flat, shallow area in the TE-TSS and the three areas that show migration (Maas West, IJgeul Approach, and IJgeul Approach anchorage) have a low correlation $\rho^{(S)}$ between time and the overall shallowest likely depth per subarea. Apparently, their overall shallowest likely depth values change independent of time.

The MESR values are also close to zero, except for the three areas that show migration. The migration makes the shallowest likely depth values at one side of the sand waves decrease. The correlation $\rho^{(M)}$ between time and the shallowest likely depth is large, except for the flat, shallow area in the the TE-TSS and the two areas in the region West of IJmuiden. For those two areas (IJgeul Approach and IJgeul Approach anchor-

Table 2: Areas per region, including codes for areas and regions used in the following Tables.

region: areas
Selected Track (ST):
Critical areas A, including Twin (ST1):
period 1991-1999 (ST1A);
period 2000-2002 (ST1B);
period 2003-2006 (ST1C)
Critical areas B, E, F, G, H, I, J (ST2);
Critical areas C, D, K (ST3);
Long Stay anchorage (ST4)
Noordhinder (NH):
Noordhinder Junction (NH1):
SBES surveys (NH1A);
MBES surveys (NH1B);
Short Stay anchorage (NH2);
Eurogeul Approach (NH3)
West of Rotterdam (WR):
Maas West anchorage (WR1)
West of IJmuiden (WIJ):
IJgeul Approach (WIJ1);
IJgeul Approach anchorage (WIJ2)
North of Terschelling (NT):
shallow part of TE-TSS (NT1)

Table 3: Averages per area for the SLDR and MESR values [m/yr], followed by their uncertainties expressed as 95% confidence limits, and correlation coefficients ρ. Positive rates mean the sea floor becomes shallower. Static areas have an average rate of exactly 0, and small rates are denoted 0.00. The region codes are given in Table 2, and the number of subareas over which the average is calculated is given between brackets. The areas Maas west anchorage (WR1), IJgeul Approach and IJgeul Approach anchorage (WIJ1-2) have MESR values that are higher than their 95% confidence limits, and are therefore marked with (!).

area (#)	SLDR	$\rho^{(S)}$	MESR	$\rho^{(M)}$
ST1A (25)	0 ± 0.05	1	0.00 ± 0.04	0.93
ST1B (25)	0 ± 0.16	1	0 ± 0.19	1
ST1C (25)	0 ± 0.10	1	0 ± 0.13	1
ST2 (20)	0 ± 0.11	1	0 ± 0.19	1
ST3 (11)	0 ± 0.08	1	0 ± 0.10	1
ST4 (32)	0 ± 0.08	1	0 ± 0.11	1
NH1A (72)	-0.12 ± 0.15	0.93	-0.04 ± 0.13	0.96
NH1B (72)	0.00 ± 0.16	0.92	0.00 ± 0.15	0.89
NH2 (24)	0 ± 0.09	1	0 ± 0.12	1
NH3 (92)	0 ± 0.09	1	0 ± 0.14	1
WR1 (18)	0.02 ± 0.04	0.28	0.12 ± 0.04	0.99 (!)
WIJ1-2 (120)	0.00 ± 0.03	0.57	0.05 ± 0.03	0.52 (!)
NT1 (14)	0.00 ± 0.01	0.15	0.00 ± 0.01	0.26

age), sand wave migration is detected, which is neither correlated with depth nor with sand wave shape. (See *Dorst* [2009].)

For the area Maas West, in the region West of Rotterdam, migration is detected that correlates with both depth and sand wave shape. (See *Dorst* [2009].) For this area, we find a large correlation $\rho^{(\mathrm{M})}$ between time and the shallowest likely depth for the nodes where the MESR is found, but a low correlation $\rho^{(\mathrm{S})}$ between time and the overall shallowest likely depth values. This difference between the migrating areas Maas West and the two IJgeul Approach areas is probably due to the less structured migration of the latter areas, as indicated by the differences in their correlations with depth and sand wave shape.

4.2 The two regularity parameters

4.2.1 The overall test quotient

An overview of the values of the overall test quotients is given in Table 4. The table illustrates that, besides the area without sand waves North of Terschelling, few overall test quotients are smaller than one, and therefore almost all subareas of the other areas are classified as irregular.

It is also clear from Table 4 that the overall test quotients strongly depend on the type of surveys: MBES surveys result in higher values than SBES surveys. The Kriging uncertainty of the SBES surveys makes their variances larger, and thereby the test quotients smaller, as they give the size of the residuals relative to the variances and covariances of the error model. Therefore, we only conclude that all subareas are irregular, but we cannot compare regions in terms of their degree of irregularity.

A third observation is that the two-dimensional overall test quotients are larger than the one-dimensional overall test quotients. The two-dimensional analysis uses the same number of depth values M to estimate fewer parameters N. This means that the estimated residuals $\underline{\hat{\mathbf{r}}}$ are larger, and thereby the overall test quotients $\underline{q}^{(\mathrm{o,m})}$ are larger as well. Only in a few cases the increase in size of the residuals is so small that the increase in redundancy $M - N$ has a larger effect on the calculation of the test quotient , and the two-dimensional overall test value is smaller. The shallow part of the TE-TSS, without a sand wave pattern, is an example of such a case.

4.2.2 The morphological variance

We see that the type of echo-sounder also influences the morphological variances $\bar{\underline{\sigma}}^{(\mathrm{m})2}$, most notably for the Noordhinder Junction. A part of the morphological variation will be incorrectly accounted for by the error variances and covariances. An error description that allows for larger residuals is able to account for more morphological variation as well.

However, another effect now dominates, which becomes clear by comparing the morphological variances of the short wavelength Critical area (A: 150 to 300 m) with those of the intermediate wavelength Critical areas (C, D and K: 200 to 400 m) and those of the long wavelength Critical areas (B, E, F, G, H, I, J: 450 to 900 m). Larger wavelengths apparently allow for larger deviations from a sine function. This difference is visible in the values for both the one-dimensional and the two-dimensional values, which confirms that this effect is caused by wave irregularity (deviation from a sine by peakedness or skewness in the x-direction), not by crest irregularity (sand wave pattern changes in amplitude or position along the y-direction).

The one-dimensional morphological variances can be both larger or smaller than the two-dimensional values. One effect has already been mentioned for the overall test quotients: the estimated residuals $\underline{\hat{\mathbf{r}}}$ are larger for the two-dimensional situation, which also means larger estimates for morphological variance. Another effect is

Table 4: Overall spatial test quotients $\bar{\underline{q}}^{(\mathrm{o,m})}$ [-] and survey-averaged estimated morphological variance $\bar{\bar{\underline{\sigma}}}^{(\mathrm{m})2}$ [m^2] per area, averaged over all subareas. The area codes are given in Table 2, and the number of subareas over which the average is calculated is given between brackets. To compare these results, the used number of SBES surveys $S^{\downarrow}$ and the used number of MBES surveys $S^{\downarrow\downarrow}$ are given as well. Both the one-dimensional grid line results and the two-dimensional grid results are given. The shallow part of the TE-TSS (NT1), marked with (*), has a one-dimensional and a two-dimensional overall test quotient larger than 1 for one subarea only, and therefore only one survey-averaged morphological variance for the one-dimensional analysis, and one for the two-dimensional analysis.

area (#)	$\bar{\underline{q}}^{(\mathrm{o,m})}$		$\bar{\bar{\underline{\sigma}}}^{(\mathrm{m})2}$		$S^{\downarrow}$	$S^{\downarrow\downarrow}$	
	1D	2D	1D	2D			
ST1A (25)	3.49	4.08	0.94	0.75	8	0	
ST1B (25)	6.15	7.49	1.03	0.91	5	2	
ST1C (25)	8.85	11.01	1.15	1.12	3	4	
ST2 (20)	5.66	7.73	3.34	3.28	6	0	
ST3 (11)	5.50	6.19	2.10	1.79	6	0	
ST4 (32)	9.43	13.18	1.81	1.86	2	1	
NH1A (72)	3.26	4.92	1.35	1.33	4	0	
NH1B (72)	21.55	31.80	2.34	3.23	0	6	
NH2 (24)	22.36	30.36	2.33	2.94	1	5	
NH3 (92)	15.13	21.91	1.56	1.92	0	7	
WR1 (18)	4.47	6.10	0.47	0.49	4	1	
WIJ1-2 (120)	6.07	9.82	0.48	0.35	4	2	
NT1 (14)	0.30	0.28	0.011	0.005	3	1	(*)

the acceptance of spatial extensions to the characterization. The larger redundancy in the two-dimensional analysis gives larger test quotients $\underline{q}_a$ for the alternative extensions a, which means that it is more likely that an extension is accepted. This implies that the estimated residuals $\underline{\hat{\mathbf{r}}}$ are smaller for the two-dimensional situation.

It depends on the crest irregularity of the area which effect dominates. For a relatively small degree of irregularity, the extra flexibility of the one-dimensional analysis does not approximate the morphology much better than the two-dimensional analysis, the estimated residuals are not much smaller. If the larger redundancy of the two-dimensional analysis is the cause of the acceptance of a spatial extension that was not accepted for the one-dimensional analysis, the two- dimensional residuals are smaller, and the size of the added morphological variance as well. For a relatively large degree of irregularity, on the other hand, the one-dimensional analysis is able to approximate the pattern much better because it is more flexible. The two-dimensional residuals are larger, and the size of the added morphological variance as well.

For example, the areas in the region West of IJmuiden have a relatively large one-dimensional morphological variance, indicating that the sand waves have a low crest irregularity. The areas in the Noordhinder region have a larger two-dimensional morphological variance, indicating a large crest irregularity. An exception are the SBES surveys of the Noordhinder Junction. The track direction usually corresponds to the x-direction of the pattern, and the interpolation procedure therefore artificially creates regular structures the y-direction of the crest. This decreases the two-dimensional morphological variance to the size of the one-dimensional morphological variance.

4.3 The two minimal detectable biases

Table 5 shows the minimal detectable biases for a depth outlier during the next survey, with a power γ of 95%. With this Table, we can now conclude from the two-dimensional MDB-s that there is no large risk of missing large-scale dynamics of a size of S44 order 1 for depth uncertainty. However, as we can conclude from the one-dimensional MDB-s, there is a higher risk that small-scale dynamics of that size will be missed for all regions, except for the region North of Terschelling.

The MDB-s are especially large for the regions Selected Track and Noordhinder, because the morphological variances of those regions are also large (Table 5), and in spite of their larger S44 critical values due to their deeper bed levels. The regions West of Rotterdam and West of IJmuiden already had a higher recommended priority, because of their MESR values. Now, we also recommend to give the regions Selected Track and Noordhinder priority over the region North of Terschelling, as indicated by a (!) in Table 5.

Table 5: Minimal detectable biases [m] for a depth outlier during the next survey, with a power γ of 95%. The area codes are given in Table 2, and the number of subareas over which the average is calculated is given between brackets. All listed details per area are averages over the subareas: measurement and interpolation variance $\bar{\underline{\sigma}}^{(e)2}$ [m^2]; number of grid nodes $\sqrt{\bar{P}}$ per grid line, assuming square grids; and number of surveys $\bar{S}$. The morphological variance $\bar{\tilde{\underline{\sigma}}}^{(m)2}$ [m^2] is taken from Table 4. The MDB-s are compared to the values for uncertainty of depth error $1.96\sigma^{(e)}$ [m] of S44, order 1, at a 95% confidence level [*International Hydrographic Organization*, 2008a]. The S44 uncertainty values are calculated using bed level $\bar{\underline{d}}^{(b)}$ [m]. The areas that were not given a higher priority in Table 3, and have a higher one-dimensional MDB than $1.96\sigma^{(e)}$ of S44, order 1, are marked with (!).

area (#)	area details				MDB		S44, order 1	
	$\bar{\underline{\sigma}}^{(e)2}$	$\sqrt{\bar{P}}$	$\bar{S}$	$\bar{\underline{d}}^{(b)}$	1D	2D	$1.96\sigma^{(e)}$	
ST1A (25)	0.40	22	6	34.5	0.96	0.19	0.67	(!)
ST1B (25)	0.41	22	5	34.5	1.01	0.21	0.67	(!)
ST1C (25)	0.18	22	5	34.6	0.97	0.20	0.67	(!)
ST2 (20)	1.05	18	6	39.4	1.92	0.45	0.72	(!)
ST3 (11)	0.49	20	6	36.0	1.40	0.29	0.68	(!)
ST4 (32)	0.14	25	3	41.2	1.16	0.24	0.73	(!)
NH1A (72)	0.67	23	4	37.1	1.19	0.25	0.69	(!)
NH1B (72)	0.12	23	6	37.6	1.27	0.31	0.70	(!)
NH2 (24)	0.12	26	6	36.0	1.19	0.26	0.68	(!)
NH3 (92)	0.11	20	6	34.2	1.12	0.27	0.67	(!)
WR1 (18)	0.08	25	5	20.2	0.59	0.12	0.56	
WIJ1-2 (120)	0.11	22	6	25.4	0.64	0.12	0.60	
NT1 (14)	0.08	16	4	19.6	0.30	0.08	0.56	

5 Results: suggested improvements to the resurvey policy

All analyzed areas under the responsibility of the Netherlands Hydrographic Service have the same resurvey category 1, with a frequency of once every two years, see Table 6. Although the analyzed areas in the region Noordhinder fall under the responsibility of Rijkswaterstaat North Sea, there are also category 1 areas of the Netherlands Hydrographic Service in this region. The two regions that have the largest dynamics with respect to the resurvey frequency are West of Rotterdam and West of IJmuiden. (See the MESR values in Table 3.) We suggest to change the current resurvey policy by assigning areas in those two regions a higher resurvey frequency than areas for which the other four factors are equal, but that are located in another region.

Also, the absence of any large indicator values for the region North of Terschelling suggest that the high

Table 6: Existing situation of resurvey categories per region. The geographic distribution of the categories over the BNLCS and the corresponding resurvey frequencies are shown in Figure 1.

region	highest current resurvey category	new priority
West of Rotterdam	category 1	2
West of IJmuiden	category 1	2
Selected Track	category 1	4
Noordhinder	category 1	4
North of Terschelling	category 1	5

Table 7: Recommended new situation: differing recommended priorities per region.

new priority	region	reason
1	-	large SLDR
2	West of Rotterdam, West of IJmuiden	large MESR
3	-	large 2D MDB
4	Selected Track, Noordhinder	large 1D MDB
5	North of Terschelling	no large indicators

resurvey frequency of the shallow part of the TSS could not be justified, unless other factors require so. The recommendations and the reasons for them are given per priority in Table 7.

6 Discussion

6.1 Shallowest likely depth as a hydrographic concept

Our concept of the shallowest likely depth is algorithmic, just like the concept of the navigation surface [*Smith*, 2003; *Smith et al.*, 2002], but the way it deals with small-scale morphology is different. Instead of defocusing isobaths around the shallowest values, we add the residual morphology to the uncertainty of the schematic characterization, and apply a depth reduction by creating a full grid of shallowest likely depth values, at a confidence level that is set as considered necessary. From such a grid, it should be possible to draw non-shoal biased isobaths that have a constant confidence level. The automatic generation of unbiased isobaths is more straightforward than the application of a defocusing algorithm, even if a scale-dependent generalization is necessary.

In a cleaned MBES survey, i.e. after the removal of gross errors and objects, the extreme values are often generated by the least accurate outer beams of the echo sounder swath. In that case, classical shoal biasing selects those least accurate values for chart production. An advantage of our concept is that it does not rely on the shallowest values, but uses a surface $\underline{\hat{m}}_{97.5\%}(x, y)$ that is estimated from all depth values and that has a specified confidence level. This reduces the importance of an advanced data cleaning procedure.

6.2 Irregularity as a morphological concept

The one-dimensional morphological variance components describe wave irregularity, without a distinction between horizontal and vertical asymmetry. Crest irregularity is included in the values of the two-dimensional morphological variance components. Crest irregularity is large if the two-dimensional morphological variance component is large, but its one-dimensional equivalent is not. Because of the relation between the morphological variance component and the MDB (equation (3.4.4) and Table 1), the MDB values contain the information on wave and crest irregularity as well. It is preferable to use the morphological variance components though, as they are not connected to a certain type of dynamics.

Knaapen [2005] found a correlation between the migration rate of sand waves in the Noordhinder region and shape information like their horizontal asymmetry. *Dorst* [2009] used the shape-based migration predictor, using the results of a two-dimensional deformation analysis. The differences between these results and results based on a one-dimensional deformation analysis are able to provide insight into the role of crest irregularity.

6.3 The four indicators

The presence of four other factors for the resurvey policy (Section 1) means that changes could only be made if the interpretation of observed sea floor dynamics (factor 5) is done in combination with the interpretation of data describing the other factors. Therefore, we make recommendations on morphological priority only, and leave the formulation of adapted resurvey frequencies outside the scope of this study.

The two indicators SLDR and MESR give a powerful combination of information on the shallowest depth in an area and the maximum shoaling rate in that area. The two MDB-s add indicators on the size of potentially missed dynamics, ensuring recommendations that are robust, even in case of complicated morphology. This enables resurvey planners to make sound choices in the assignment and change of resurvey frequencies, leading to safer navigation and more efficient deployment of survey capacity.

The sand wave pattern in all four sand wave regions is irregular (See the overall spatial test quotients in Table 4.), i.e. the pattern differs from a one-dimensional

sine function that is constant in the direction along the crest. The two regions with migrating sand waves are less irregular, and the two regions without migrating sand waves are more irregular (See the morphological variances in Table 4.). Potentially, smaller dynamics are not detected in these areas. Change of survey frequency of the two more irregular regions, based on the generally static results of the deformation analyses of those regions, should therefore be done with care.

7 Conclusion

The results of the deformation analysis, applied to bathymetric surveys in the Southern North Sea, have been interpreted using four indicators. These indicators are the Shallowest Likely Depth Rate (SLDR), the Maximum Estimated Shoaling Rate (MESR), and the Minimal Detectable Biases (MDB-s) for the one-dimensional and the two-dimensional analyses. They summarize the estimates for the morphological parameters, and thereby finalize the data reduction in several steps, starting with a series of survey data. The irregularity of the analyzed patterns differs, which gives different sizes of dynamics that are detectable.

In the present survey policy, all analyzed areas fall into the category with the highest resurvey frequency, or fall under the responsibility of Rijkswaterstaat North Sea. Using the indicators that we developed, the regions of the analyzed areas are ordered into several categories. The regions West of Rotterdam and West of IJmuiden should have a higher priority than the regions Selected Track and Noordhinder, which in turn should have a higher priority than the region North of Terschelling. (Also see the Tables 6 and 7. This contributes to the efficiency of the survey efforts that the Netherlands Hydrographic Office makes in the regions of the analyzed areas, making more time available to survey other areas. This in turn aids safe navigation in the Southern North Sea.

The approach to improve the resurvey policy by the analysis of a series of data is possible due to the storage of past surveys at a high resolution. The resulting recommendations for the survey plan are of higher detail than recommendations from exploratory surveys or remote sensing techniques. With the recent improvements in morphological models, these models could also become a valuable source for adaptations in resurvey frequency, especially in cases where future human intervention plays a role.

Acknowledgments

The sources of the used data are the Netherlands Hydrographic Service and the North Sea Directorate of Rijkswaterstaat, available as part of their co-operation in the Netherlands Hydrographic Institute. Both organizations are gratefully acknowledged.

An earlier interpretation of the results was done by *Huizenga* [2008]. The interpretation done in this paper is based on his graduation report. The authors thanks Bregt Huizenga for his useful exploratory work. The authors acknowledge the staff at the Netherlands Hydrographic Service, for giving direction to this research project, and their support in the creation of the paper. This project has been co-sponsored by the Technology Foundation STW, the applied science division of NWO, and the technology program of the Dutch Ministry of Economic Affairs.

References

Besio, G., P. Blondeaux, M. Brocchini, S. J. M. H. Hulscher, D. Idier, M. A. F. Knaapen, A. A. Németh, P. C. Roos, and G. Vittori (2008), The morphodynamics of tidal sand waves: a model overview, *Coastal Engineering*, *55*, 657–670, doi: 10.1016/j.coastaleng.2007.11.004.

Burton, B. W. (1977), An investigation of a sandwave field at the south western end of Sandettié Bank, Dover Strait, *Int. Hydro. Rev.*, *54*(2), 46–59.

Calder, B. (2003), Automatic statistical processing of multibeam echosounder data, *Int. Hydro. Rev., New Series*, *4*(1), 53–68.

Calder, B. (2006), On the uncertainty of archive hydrographic surveys, *IEEE J. of Oceanic Engineering*, *31*(2), 249–265, doi: 10.1109/JOE.2006.872215.

Calkoen, C. J., G. H. F. M. Hesselmans, and G. J. Wensink (1998), The use of radar imagery to assess the bottom topography of shallow seas, *Int. Hydro. Rev.*, *75*(2), 43–50.

De Oliveira, S. S., F. Mandarino, and F. J. De Souza (2007), FIS: resurvey decision system — using fuzzy inference systems for area selection, *Hydro Int.*, *11*(3), 31–34, available at: www.hydro-international.com.

Dehling, T. (2006), Determining survey frequency and resolution — BSH concept and realisation, *Hydro Int.*, *10*(2), 7–9, available at: www.hydro-international.com.

Deltares (2008), Research design for the scientific validation of the hydrographic survey policy of the hydrographic office of the royal netherlands navy, *Tech. rep.*, Deltares, Subsurface and Ground water systems department, Utrecht, The Netherlands.

Dienst der Hydrografie (2007), Risicoanalyse achterstanden hydrografische opnemingen, peildatum 1 oktober 2007, *Tech. rep.*, Hydrographic Service of the Royal Netherlands Navy, The Hague, The Netherlands.

Dorst, L. L. (2009), Estimating sea floor dynamics in the southern north sea to improve bathymetric survey planning, Ph.D. thesis, University of Twente, Enschede, The Netherlands, no. 69 in Publications on Geodesy, Netherlands Geodetic Commission, ISBN: 978-90-365-2878-8 and 978-90-6132-311-2, available at: www.ncg.knaw.nl.

Dorst, L. L., P. C. Roos, S. J. M. H. Hulscher, and R. C. Lindenbergh (2009), The estimation of sea floor dynamics from bathymetric surveys of a sand wave area, *J. of Applied Geodesy*, *3*, 97–120, doi: 10.1515/JAG.2009.011.

Heap, B. (2007), Mariner perceptions regarding the display of uncertainty on nautical charts, Master's thesis, University of New Hampshire, Durham, USA.

Huizenga, B. (2008), The interpretation of seabed dynamics on the Netherlands Continental Shelf, Master's thesis, University of Twente, Enschede, The Netherlands.

International Hydrographic Organization (2007), IHO transfer standard for digital hydrographic data, *Tech. Rep. Special publication 57*, International Hydrographic Bureau, Monaco, available at: www.iho.int.

International Hydrographic Organization (2008a), IHO standards for hydrographic surveys, *Tech. Rep. Special publication 44, 5th ed.*, International Hydrographic Bureau, Monaco, available at: www.iho.int.

International Hydrographic Organization (2008b), Status of hydrographic surveying and nautical charting worldwide, *Tech. Rep. Special publication 55, 3rd ed.*, International Hydrographic Bureau, Monaco, available at: www.iho.int.

Kember, I. D. (1984), How often? — towards an optimum survey interval for mobile seabeds, *Int. Hydro. Rev.*, *61*(1), 55–79.

Knaapen, M. A. F. (2005), Sandwave migration predictor based on shape information, *J. Geophys. Res.*, *110*(F04S11), doi: 10.1029/2004JF000195.

Langeraar, W. (1966), Sand waves in the North Sea, *Hydrogr. Newsletter*, *1*(5), 243–246.

Le Bot, S., D. Idier, T. Garlan, A. Trentesaux, and D. Astruc (2000), Dune dynamics: from field measurements to numerical modelling — application to bathymetric survey frequency in the Calais-Dover straight, in *Proceedings of the international workshop on Marine Sand Dynamics, Lille, France*, edited by A. Trentesaux and T. Garlan, University of Lille 1, Lille, France.

Németh, A. A., S. J. M. H. Hulscher, and R. M. J. Van Damme (2007), Modelling offshore sand wave evolution, *Continental Shelf Res.*, *27*, 713–728, doi: 10.1016/j.csr.2006.11.010.

NOAA Office of Coast Survey (2008), NOAA hydrographic survey priorities, *Tech. rep.*, National Oceanic and Atmospheric Administration, available at: www.nauticalcharts.noaa.gov.

Roos, P. C., S. J. M. H. Hulscher, and H. J. De Vriend (2008), Modelling the morphodynamic impact of offshore sandpit geometries, *Coastal Engineering*, *55*, 704–715, doi: 10.1016/j.coastaleng.2008.02.019.

Smith, S. M. (2003), The navigation surface — a multipurpose bathymetric database, Master's thesis, University of New Hampshire, Durham, USA, available at: www.opennavsurf.org.

Smith, S. M., A. Alexander, and A. A. Armstrong (2002), The navigation surface: a new database approach to creating multiple products from high-density surveys, *Int. Hydro. Rev., New Series*, *3*(2), 12–26.

Su, H., H. Liu, and W. D. Heyman (2008), Automated derivation of bathymetric information from multi-spectral satellite imagery using a non-linear inversion model, *Marine Geodesy*, *31*, 281–298.

Swart, L. M. T., J. Vogelzang, G. J. Wensink, P. Groenewoud, L. F. G. M. Hendriks, N. Nass, and W. T. B. Van der Lee (2006), Towards implementation of the BAS within Rijkswaterstaat, *Tech. Rep. AGI-2006-GAB-003*, Ministry of Transport, Public Works and Water Management of the Netherlands, Rijkswaterstaat, Delft, The Netherlands, available at: www.swartvast.nl.

Van der Veen, H. H. (2008), Natural and human induced seabed evolution — the occurence of large-scale bed patterns and the effects of human activities on the North Sea seabed, Ph.D. thesis, University of Twente, Enschede, The Netherlands, ISBN: 978-90-365-2613-5, available at: doc.utwente.nl.

Whatrup, C., D. Mann, and B. Davidson (2005), The UK civil hydrography programme — changing the mould, *Int. Hydro. Rev., New Series*, *6*(2), 45–56.